High Gain Photodetectors formed by Nano/Micromachining and Nanofabrication

David R Winn, *Member, IEEE*

Abstract– **Recently available methods in highly anisotropic nano/micromachining and nanofabrication (N/MEMS) enable the fabrication of high gain photodetector structures in both vacuum and semiconductor optoelectronics. We show results on nanomachined microchannels formed in semiconductors which enable robust long life photomultiplier-like tubes scaling in diameters from less than 1 mm to 30 cm in diameter, in various shapes (like strips or hexagons) with very compact dimensions along the axis, well less than 1 cm in thickness. The gain lifetime exceeds 1 C per square cm, and the gains can exceed 9,000 per nanomachined channel. The photolithographically precise channels enable precision imaging. Because the base matrix is a purified semiconductor, very low self-radioactivity counts result, unlike Pb-glass MCP. Additionally, because of the absence of lead, as in lead-glass MCP, common vacuum photocathodes can be deposited directly on the throats of the microchannels. We also show deposition on the throats of the the microchannels B-doped diamond with a SE yield exceeding 100, for photon counting. We also discuss results on a photodetector using a method akin to field emission into silicon, giving an APD-like gain using the geometric shape of the electrodes rather than doping profiles to achieve a controllable high field avalanche-gain region, with a considerably lower noise than compensated doped APD, also as a result of a high field volume, the major noise source, reduced by about 1000 times compared to equivalent APD. This gain has been tested in single pixel formats using AFM tips as the basis for the detector, and exceeded 5,000 in Geiger mode. These high gain pixel-sized detectors can be formed into imaging chips or silicon-PMT-like gained pixel array devices. We discuss applications in a wide variety of scientific instrumentation.**

I. Introduction

Photomultiplier tubes (PMT) are used in a wide variety of high energy detectors, including scintillating fiber arrays, calorimeters, Cerenkov and RICH counters, trigger counters, beam monitors and others. PMT have changed slowly in the last decades, as have glass-based MCP-PMT which have demonstrated ability to operate in high magnetic fields with superior time resolution. Vacuum based photomultiplier (PMT) technology represents one of the most versatile photosensitive devices available. Photomultipliers provide high sensitivity (single quantum) and ultra-fast high gain response compared to other photosensitive devices. Existing PMT have bandwidths (BW) up to 2 GHz at gains of $10^{5\text{-}6}$. At lower BW, gains exceeding 10^9 are possible. Photocathodes can have sensitivities covering wavelengths from ~200nm - 1.8 microns. Miniaturization of traditional photomultipliers from typical photocathode sizes of ~1 cm diameters down through sub-mm (down to fiber diameters) sizes represents an evolution of this traditional light detection technology. However, PMT's are relatively bulky, expensive, often largely hand-assembled vacuum tube devices that haven't changed significantly in the last few decades, with minimal flexibility on the volume or shape of the sensitive region. Typically the volume exceeds ~(1-2) x D^3, whereas we propose a PMT that scales more like <0.3 x D^3 where D is the cathode major diameter. Time response can only be improved to the 10 GHz regime if the electron trajectories are constrained and shortened. Further, to obtain large area position sensitivity, tiles or arrays of PMT's must be used, especially if the cross-talk inherent in a multianode PMT must be avoided. Innovative advances to the design and fabrication of PMT's would provide useful detectors with spatial resolution as fine as ~0.05 mm, with zero pixel-pixel cross-talk, sub-nanosecond risetimes, timing jitter less than 20 ps, counting rates exceeding 5 GHz with low gain-shift (able to take advantage of modern low-cost multi-GHz counting electronics), quantum efficiencies up to 50% in the UV-visible, single-photon pulse-height resolution better than 10%, all in the same or similar suites of devices.

Moreover, reducing the volume of the detectors by a significant amount will enable high-density packaging for complex detectors such as those used in complex calorimeters, fiber trackers (or, for example, dark matter search spectroscopy, nuclear spectroscopy, PET imaging, and so forth). As an example, this technology enables a standard 2" PMT performance in a package 2" in diameter (or square or hexagonal) x less than 3-4 mm deep (thick to the photon beam). This technology is scalable in photocathode area and photocathode shape without major modifications. The technology is particularly well-adapted to tiling with minimal dead area between elements, and by enabling a wide variety of shapes (squares, hexagons, octagons for example).

Miniaturization and especially micromachining of photomultipliers has many technical advantages for detection system developers such as:

- Faster response times with lower time jitter, due to decreased electron path-lengths. The jitter of a PMT with a 0.5 mm photocathode/dynode assembly is estimated to be less than 10 ps, with a BW of 10 GHz at a gain of 100,000.

Manuscript received November 23, 2007.
This work was supported in part by the U.S. Department of Energy.
D. R. Winn is with Department of Physics, Fairfield University, Fairfield, CT 06824-5195 e-mail: winn@mail.fairfield.edu; Telephone 203.254.4000

- Surface mountable detectors directly interfacing to high-speed electronics, together with very high density anode vacuum feedthrough connections.
- Tileable detectors with minimum lost area, and very dense arrays
- In some realizations, essentially no cross-talk, in contrast with typical multi-anode PMT where 5% cross-talk (or more) is typical.
- Imaging is possible at gains of 10^6 at 2 GHz, with sub-mm pixels.
- Cost- effective, lower cost manufacturing through adaptation of semiconductor manufacturing procedures that enable higher throughput.
- Very large PMT with flat windows may result, since the dynodes and interdynode insulators form a rugged stack capable of supporting a window directly.
- Ultra-fine MCP channels, up to ~ 1-2 x 10^5/mm^2 enable high rates, despite individual microchannels paralyzed for a few microseconds.
-

But several basic problems exist with glass MCP used in PMT: a) the materials of the Pb- or other heavy metal containing glasses poison photocathodes, when released by electron bombardment; b) relatively weakly bound water, oxygen and hydrogen contained in all convenient glasses yield ion production under electron bombardment, which degrade the MCP, cause afterpulsing, and photocathode damage, leading to short PMT lifetimes compared with metal-oxide dynode and short gain-lifetime at high incident electron fluxes[[i]] ,[[ii]]; c) the glass MCP processing is expensive, requiring pulling a softened glass boule of etchable core glass fibers, d) Spatial defects due to the fiber-bundling process lower the effective spatial resolution and image uniformity and limit the ability to couple the MCP to silicon-device readout e) in glass, the limiting the diameter of convenient or cost effective MCP to sizes less than 2"-3" diameters and very expensive PMT for comparable sizes to dynode PMT; f) Glass MCP suffer from operation and fabrication at relatively low temperatures (precluding most CVD activation or brazed mountings), evolution of hydrogen ions from the surface (potential photocathode degradation); g) pixel sizes are usually larger than ~5-6 μm for commercially viable products; h) relatively low pore areal packing fractions (<60%-65% open pores) create an upper limit on detection efficiency, near this areal open fraction; i) glass MCP are self-radioactive and non-radiation-hard at levels incompatible with some very low-light or space applications. We have therefore looked at silicon micromachining to develop a new type of Si- and quartz-MCP materials systems, which can take advantage of the mass production technologies developed by the semi-tool and semiconductor industry.

II. Applications of N/MEMS to Vacuum Photodectors

The techniques of N/MEMS, micromachining, and silicon foundries have been used to produce micromachined all silicon PMT assembly, using silicon and quartz wafers (and/or silicon converted to amorphous quartz or silicon carbide by oxidation or carburizing after micromachining) capable of being assembled into ultra-compact PMT capable of high B operation, superior time resolution, long lifetimes, and diameters up to 12"(30 cm). In advanced realizations, the separate vacuum envelope is eliminated by including a vacuum wall section in the machined dynodes. A thin SiMCP stack results, typically <1mm per plate, well within the breakdown voltage used in semiconductor technologies of 10 V/mm. Additionally, minimal wall thickness between PMT results, and arbitrary shapes and anode pixellation is possible. Thus we propose to not only more fully automate the manufacture of PMT resulting in low cost and high yields, but to produce PMT with significant performance, form, fit and function enhancements, including:

- Compactness: Minimal volume for a given photocathode area – the thickess to the beam of the gain mechanism including window and anode is less than 5 mm thick;
- High-B Operation*:* Since the electrons are proximity-focussed, channelized and extremely compact dimensions, operation in magnetic fields parallel to the PMT axis is contemplated, much like mesh or MCP PMT.
- Photocathode Sizes: Sizes scaled between sub-mm diameter (single fiber readout) up to, say, 30 cm diameter x 8mm thick flat "dinner plate" tubes for large neutrino, cosmic ray or proton decay detectors. In the case of both small and large diameter PMT, the electrode structures can become structural elements which support the window and the anode and form the side vacuum wall, and transfer the pressure load to the entire structure, thus enabling flat windows in large sizes, and very thin windows in small sizes. It is estimated that a window of 50-100 mm thickness is sufficient for a 1x1 cm PMT.
- Ultra-fast Timing: Because the electron trajectories are highly spatially defined, and very short compared with typical PMT, the transit time through a stack of micromachined MCP 1-2 mm thick is less than 100ps, and the concomitant time jitter less than that, typically <10% of the transit time. A 10GHz BW is possible, as scaled from existing 2GHz BW PMT, assuming similar inductance of the anode on a 1cm diameter PMT (~0.2 mH).
- Multi-Anode Arrays: because the electrons are fully channelized, imaging PMT with anodes (as bump bond points to match to a pixel readout-chip) as small as 50 micron on centers is possible with this technology. We have demonstrated vacuum metal feedthrus of 6 micron wide nickel wires on 8 micron centers (a so-called "z-axis connector") through amorphous quartz "microchannel" plates. These multianode arrays could be in the form of 2-D arrays, or 1-D arrays for reading fiber ribbons; using this technology, a PMT 2-3 mm wide x 10.3 cm long with a linear strip of 100 1x1 mm pixels, only 5 mm thick can be envisioned.
- Shape and Boundaries: Custom photocathode shapes, including strips, stripes, rectangles, hexagons, or other desired configurations; Small edge-edge

boundaries for tiled arrays, with a boundary as low as 1 mm between PMT.

- Ruggedizable: The dynode structure and the vacuum structure ultimately become fully integrated in this PMT design. The SiMCP, machined from silicon plates, and using thin and thick film deposition of insulators and conductors can become structural elements, and thus do not suffer from vibrational constraints which require special PMT for space-flight, for example.
- Single-PE resolution: thin cesiated B-doped diamond-coated dynodes show a gain of 25 at 300V, and the Si surfaces of the micromachined dynodes proposed are ideal for this purpose.
- Cost Benefits: By using standard silicon Fab & MEMS technologies, much of the "hand-labor" still used in PMT assemblies is largely eliminated.

Miniaturization of photomultiplier technology dramatically expands the realm of applicability, enabling imaging, portable and more compact detector/instrument applications. Additionally, finely pixellated PMT enable fiber readouts and other imaging applications (RICH, and others). On the other hand, large PMT have a wide variety of applications in low rate/low cross section experiments in neutrino & astroparticle physics.

III. Progress in MicroMachined Silicon Microchannel Plates for MicroMachined PMT

Microchannel plates (MCP) fabricated from standard silicon wafer substrates using a novel silicon micromachining process, together with standard silicon photolithographic process steps, have been fabricated[iii]. The resulting SiMCP microchannels have dimensions of ~0.5 µm up to ~25 µm, with aspect ratios up to 300, and have the dimensional precision and absence of interstitial defects characteristic of photolithographic processing, compatible with positional matching to silicon electronics readouts. The open channel areal fraction and detection efficiency may exceed 90% on plates up to 300 mm in diameter. The resulting silicon substrates can be converted entirely to amorphous quartz (qMCP) or SiC. The strip resistance and secondary emission are developed by controlled depositions of thin films, at temperatures up to 1,200°C, also compatible with high-temperture brazing, and can be essentially hydrogen, water and radionuclide-free. Novel secondary emitters and cesiated photocathodes can be high-temperature deposited or nucleated in the channels or the first strike surface. Results on resistivity, secondary emission and gain are presented below.

Silicon MCP Substrates: Silicon microchannel plates (SiMCP) have been fabricated using a photolithographically initiated proprietary micromachining process developed at NanoSciences Corporation (NSci). The placement, size and pore uniformity of the silicon MCP substrate channels therefore have dimensional precisions greatly exceeding that of glass-fiber-based MCP. Figures 1-4 show SEM micrographs of 4 different forms of these substrates, and Figures 5a-c show optical photographs of the SiMCP. The complete elimination of MCP defects (for example, due to misplacement or defomation of the glass fibers in a boule) is achievable, and the microchannel outputs can be placed with precision with respect to potential lithographically patterned readouts. Pore diameters are fully adjustable between 0.5-25 µm, with high aspect ratios (α=hole length/hole diameter) - up to 300:1 has been achieved with 3 µm holes - a possible theoretical limit is α>2,000:1. Large SiMCP diameters are possible, up to the size of available silicon wafers - limited with presently commercially viable silicon wafers to ~30 cm (12") diameter SiMCP plates. At present, SiMCP of 10 cm diameter have been produced, limited only by the installed photolithographic equipment (4" wafer fab). The holes can be square, and >90% open area; micromachining can taper the hole entrances as shown in Figure 1. These SiMCP substrates can be vacuum-baked at temperatures ~1,200° C, and brazed at similar elevated temperatures, much hotter than those possible with glass MCP, or converted entirely or partially to oxide (amorphous quartz - qMCP) for even higher temperature processing. Chevroning up to 8° to the surface plane have been demonstrated, as shown in Fig.4.

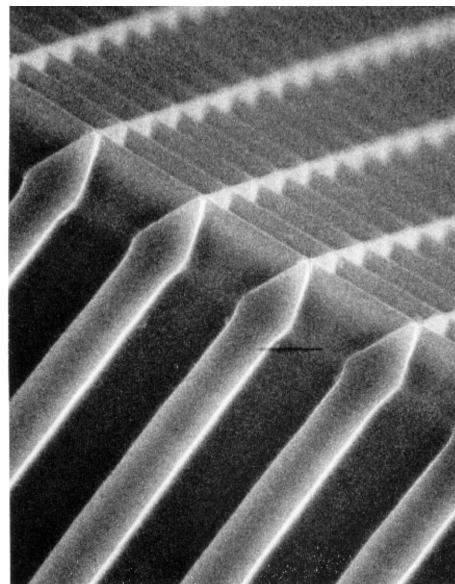

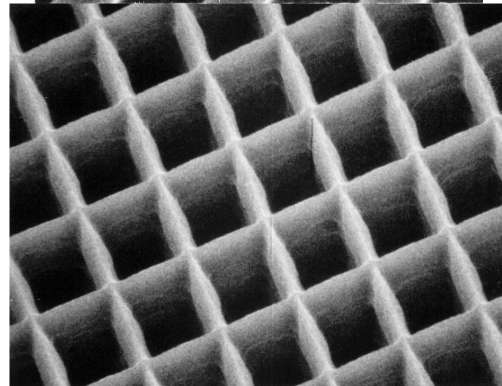

Fig. 1a,b: Micromachined Silicon Plates for a precision Si MCP Photomultipliers: The square channels are on a 6 µm spacing, with a side dimension of 3 µm. The top surface has been micromachined to a tapered blade point to enhance the collection efficiency of incident photoelectrons; approximately 95% of the surface is open, with an aspect ratio of 80:1. The Si MCP is steam oxidized to SiO2, and then used in PMT for: a) for insulator standoffs for channelized photo & secondary electrons (when coated with a resistive film) between dynodes, photocathode and anodes; b) when filled with metal wires (electroplating), they serve as a vacuum feedthru/"z-axis"

mass connector on the micro-scale, ultimately for connection to a pixel readout-chip; and c) serve as directly MCP gain stage when processed with conductive and SE films. SiMCP as large as ~30 cm can be fabricated from standard 12” Si wafers.

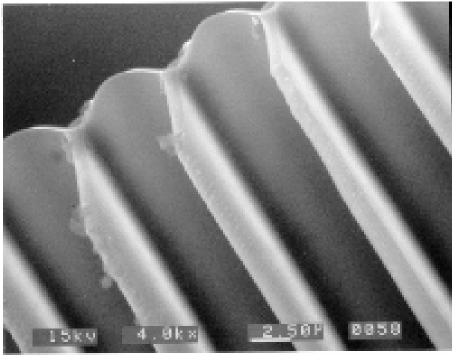

Figure 2: Cross-section views of a section of an extremely thin-wall silicon SiMCP substrate converted to amorphous quartz. Note that the walls in the channels are extremely smooth; more than 90% of the silicon is removed. Fiducial bar=2.5 microns.

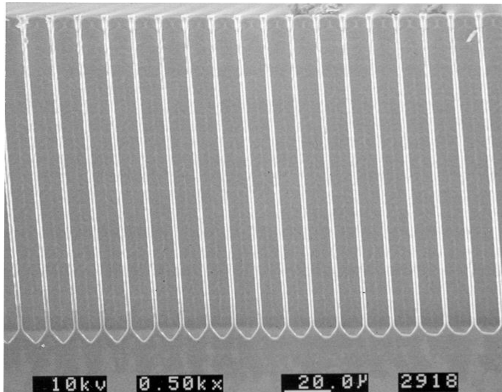

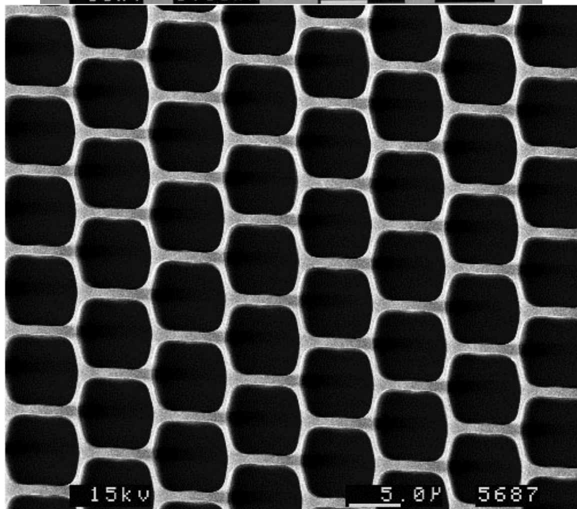

Figures 3a,b: Quasi-hexagonal Channels: Elevation and Plan views of a partially completed p-type silicon wafer SiMCP substrate using high aspect ratio silicon micromachining processes. The 10 µm on 11.25 µm pitch SiMCP channels are chevroned at about 8° to the wafer surface plane.

Electrical Isolation, Strip Resistance, and Secondary Emission Coatings Because of these temperature characteristics and the silicon-based substrate, CVD processes can be used to activate the SiMCP or qMCP plates with anhydrous, high temperature secondary-emission materials or with photocathodes. Since silicon is semiconducting and has a relatively small band gap ~1.07 eV, it is not possible to develop high enough electric fields in the channels for generating electron gain. Even for intrinsic silicon whose resistivity is ~10^4 Ω-cm, the resistance of a 1 square cm, 0.36 mm thick plate silicon MCP having 6 µm square channel openings on 8 µm centers, α = 60 (for example), would draw aboout 1,200 W at 1 KV. Therefore, bare silicon plates cannot be used due to excessive conductivity.

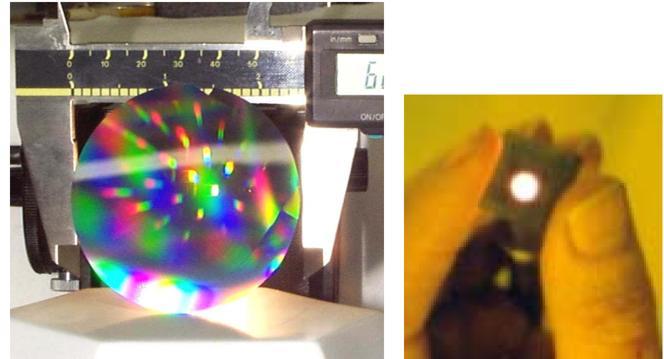

Figures 4a,b: Photographs of a 4” flash-illuminated mcp showing the diffraction pattern from the holes. And a Diced-out 1cm x 1 cm SiMCP section, back-illuminated with a spotlight.

A strategy of coating the silicon with an insulating coating, then a strip resistance layer and then a secondary emission layer has been employed to circumvent this problem. A schematic diagram of the coatings necessary for reproducing the functionality of the reduced lead glass microchannel plate surface is shown in Figure 6. The insulating layer provides the isolation necessary to keep the generated secondary electrons from being shunted by the conducting silicon substrate. The strip resistance is a weakly conducting layer that re-supplies charge to the secondary emission layer to maintain the secondary electron gain.

The isolation layer strategy was initially discussed by Tasker et al. [iv],[v] in the development of silicon based MCP and as for coatings for single channel multipliers. They developed a successful coating system for quartz tube single channel multipliers that employed a slightly oxidized polysilicon layer that provided both the strip resistance and secondary emission surface.

Electrical isolation and strip resistance of the silicon MCP is accomplished using a two step isolation procedure. Since the Si-MCP substrate is conductive, the strip resistance layer must first be insulated from the Si substrate as illustrated in Figure 6. The isolation can be accomplished by thermally oxidizing the Si-MCP substrate and/or depositing an insulating layer. The insulating layer thickness depends on the bias voltage stand-off required. After the SiMCP substrate wafer has been diced into the desired SiMCP shapes, they are inserted into a high temperature wet oxygen oxidation furnace to grow a thick (~1 µm or more) oxide layer on the top surfaces of the outer frame of the device as well as on the walls of the channels in the device. Special post-processing deposition is also used to form a frame for mechanically handling the SiMCP, whilst maintaining surface flatness. The silicon

oxiding can be complete, forming a quartz MCP (qMCP), or partial, preserving an optically opaque channel wall (other applications).

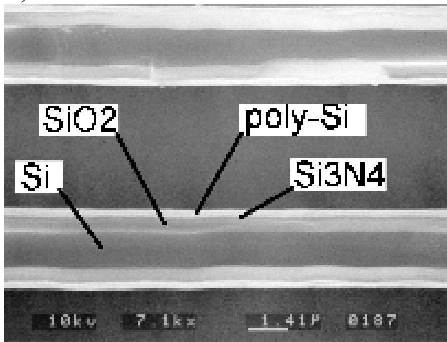

Figure 5: Cross-sections through a single channel wall of a fractured, processed SiMCP plate showing the thermal oxide and CVD-deposited polysilicon, thick silicon nitride and SiO_x coatings in the SiMCP structure.

The strip resistance for single channel electron multipliers that are typically ~1 µm in diameter and ~60 µm in length needs to be ~10^8 Ω's [iv],[v]. For a strip resistance layer ~0.1 µm in thickness, the resistivity needs to be ~50 Ω-cm, a value that is straight forward to obtain by chemical vapor deposition. In contrast, for example, a square cm SiMCP of 6 µm square microchannels on 8 µm centers, 360 µm long with a ~0.1µm thick strip resistance layer, requires the polysilicon layer to have a resistivity of ~10^8 Ω-cm since the resistance of the individual channels are all in parallel with one another. Polysilicon can be deposited having resistivity over the range 1-10^7 Ω-cm using plasma chemical vapor deposition[vi], reactive sputtering [vii] and electron beam evaporation[viii]. Coatings based on CVD techniques are desired since uniform coatings can be produced on channels of high aspect ratio. It is possible to deposit very high resistivity amorphous Si and extremely fine grain polysilicon films by CVD, and doping with nitrogen and/or oxygen. Films having resistivity on the order of 10^{10} Ω-cm have been achieved using the thermal decomposition of dichlorosilane in ammonia at temperatures ~850 C. Uniform coatings are also readily achieved on high aspect ratio channels L/d > 60 employing low pressure deposition atmospheres ~10 to 500 mTorr.

A cross-section through a wall of some processed Si-MCP are shown in Fig. 5. The cross-section shows the Si core that remains after partial thermal oxidation, and the polysilicon coating that provides the strip resistance. The oxide was grown by thermal oxidation in a flowing atmosphere of water vapor in oxygen [ix]. The polysilicon can also be doped with nitrogen; a thin deposit of silicon nitride helps enable the smooth nucleation of the polycrystalline Si/SiO_x film on the SiO_2 layer.

Secondary emission is obtained from thin films of SiO_2 and SiO_x (as in normal lead glass MCP) although CVD nucleating on silicon, silicon dioxide or silicon nitride offers many other high performance alternative SE materials systems, such as silicon silicides, metal oxides, diamond, GaP or cesiated semiconducting materials, to be described elsewhere. An optimized 10 nm thick Si/SiOx film will reach a peak SE yield of 3.5-4 betweeen 300-400 eV incident [x],[xi],[xii]; the thin SE films deposited to date exhibit the expected SE behavior vs incident electron energy.

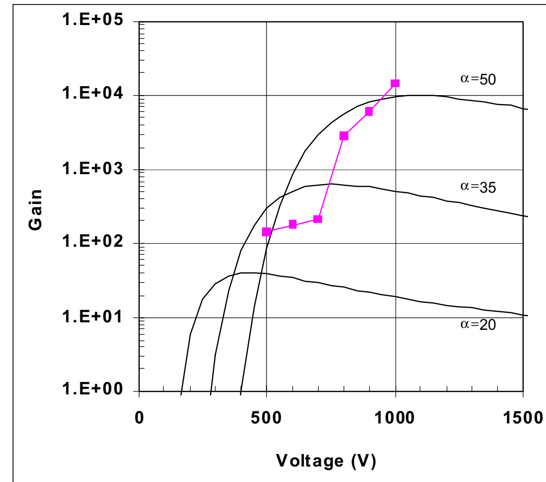

Figure 6a: Electron gain measured as a function of applied voltage for a single silicon microchannel in a SiMCP with an aspect ratio α=50 (squares), obtained in an electron microscope. Solid lines are theoretical calculations of gain for SiMCP having aspect ratios of α=50, 35, and 20.

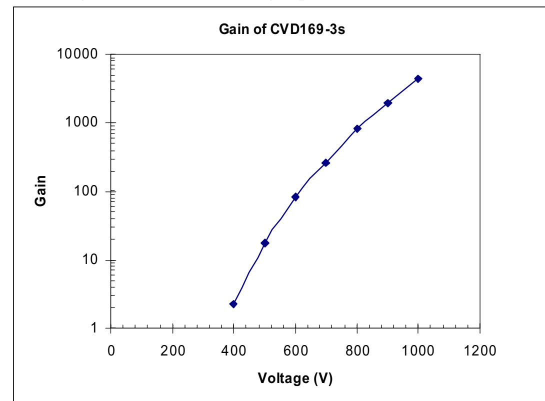

Figure 6b: Gain measured as a function of voltage applied to Si-MCPs. Square channel openings ~6 mm spaced on 8 mm centers, aspect ratio is ~60:1. Gain is over 5,000 at 1,100 V.

The gain in a silicon microchannel of a SiMCP has been measured using an electron microscope electron beam and is shown in Fig. 6 compared with theoretical values calculated from the applied voltage, measured SE yield data, and the pore aspect ratio α as:

$$G = (AV/2\alpha V_o^{1/2})^\gamma \quad (1)$$

with $$\gamma = 4\alpha^2(V_o/V) \quad (2)$$

and A given by the SE yield data δ from:

$$\delta = AV_c^{1/2}, \quad (3)$$

and V is the total channel voltage, V_o is the initial energy of the secondary electron,~ 1 eV. (The gain may be somewhat low due to saturation from using an SEM electron beam for the incident electrons.

Lifetime and Reduced Radioactive Background: The absence of water or hydrogen in the SiMCP materials system helps with electro-optic device longevity (especially the photocathode) when using these silicon-based MCP, in contrast to glass-based MCP. Note in Fig. 7, the gain actually increases with drawn charge, exactly the opposite of glass MCP. SiMCP are repeatably able to cycle between air and

vacuum with little change in performance. Measurements using a residual gas analyzer have shown that the Si plate outgases to the same level as a glass MCP in 400 seconds, compared with 15,000 seconds for the glass MCP. Moreover, the self-radioactivity of glass MCP from K and other isotopes is shown to be reduced by a factor of 20. The silicon can also be fully oxidized to amorphous quartz, for SE activation processing or strip resistance processing up to 1,400° C.

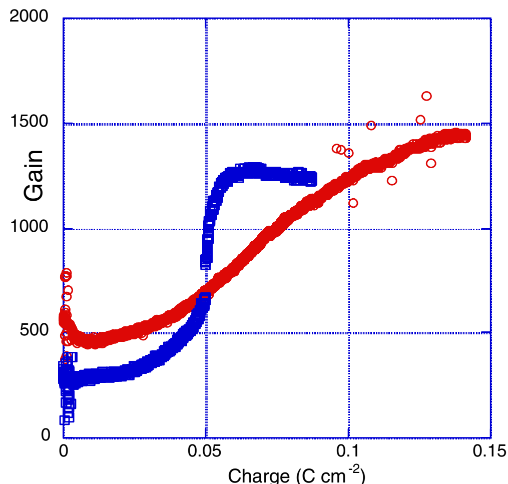

Fig.7: The plot shows MCP gain as a function of extracted charge, for two Si MCP's. Note the gain *increases*, the *opposite* of glass MCP's, due to the initial scrubbing of adsorbed water and oxygen in early stage. We emphasize that this enables SiMCP PMT with lifetimes approaching that of dynode PMT.

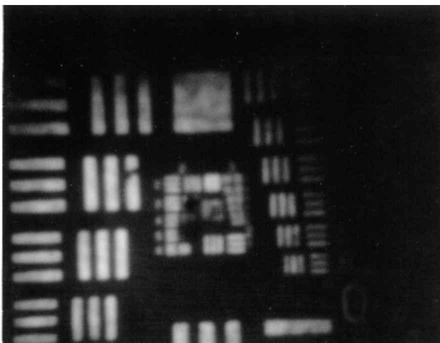

Figure 8: Test image tube structure for silicon MCPs. The picture shows the image of the standard Air Force test pattern at the output of the tube. These results show that the silicon MCP is capable of resolving >100 line pairs/mm (limited at present by the readout screen), higher than glass MCP.

Image Tube: A silicon MCP has been installed in a cesiated photocathode imaging tube, and have demonstrated spatial resolution of at least 89 lp/mm - limited by the resolution of the readout. Fig. 8 shows a tube assembly and the imaged test pattern.

Direct Photocathode Deposition on the MCP throats and High-B Operation: An important feature of SiMCP or qMCP substrates are that they are fully temperature and especially chemically compatible with cesiated cathodes fabricated directly on the surface or walls of the MCP substrate (see Figs 1 & 2), unlike leaded-glass-based MCP (the glass materials necessary for a SE glassy surface, particularly Pb glass, poison most cesiated photocathodes), which would enable; a) very high magnetic field operation, as the photoelectrons would be confined to the microchannels, and b) very low cross-talk as the window could be self-supported on the MCP and vanishingly thin (50 micron quartz sheets) and the p.e. are channelized, and c) a performance and/or cost advantage in many applications. An estimate of the strike probabilities estimates operation up to 5T is possible with 10 micron channels.

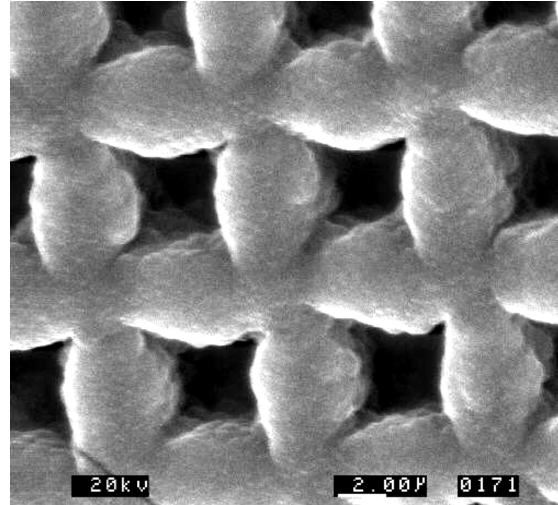

Figure 9: Diamond surface deposits on Si-MCP substrates to enhance first strike gain. The SEM photo shows a plan view of the coated substrate.. At 1-2 kV, the boron-doped diamond has gain between 60-80.

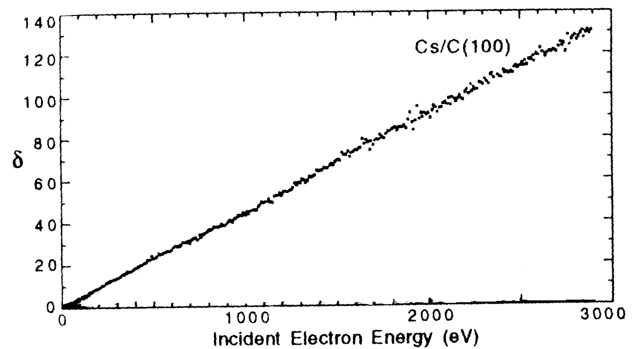

Figure 9: Potential for Diamond Dynodes: At 2000 V K-D1 appropriate for a proximity-focused PMT for High-B operation - the secondary yield for B-doped diamond exceeds 120 e per electron.

Diamond SE Deposition Figures 9 show the remarkable potential for such diamond film deposition using diamond CVD technology (a thermal dissolution of low pressure methane/hydrogen). A diamond film can produce SE emission yields well above 100, for better than 10% resolution on 1 p.e.

IV. Geometric APD using Nanomachining

APD's are reverse biased photodiodes that can achieve gains of a ~million in the Geiger mode, but without any proportionality (no dynamic range) to the light signal, and gains of several hundred up to 1,000 in the proportional mode, with a useful but limited dynamic range of ~100. APD use a high field region in a junction obtained by a high resistivity doping profile, where the carriers (typically electrons) are accelerated to high enough velocities that impact ionization occurs several times, producing avalanche gain before they leave the high field region. The limited Geiger discharge is

quenched when the reverse bias voltage (in effect, the electric field) falls below breakdown, via an effective bias/decoupling resistor ($R \sim 10^5$ Ohms) built in to the APD structure, which also decouples the individual pixels from each other, preventing neighbor pixels from discharging, since $C_{pixel}R_{pixel} > 10^{-8}$s >> 1 ns > $t_{discharge}$. The gain g per accelerated free electron (from absorbed photons or noise) is given by the charge Q storable in the pixel of capacitance C and the charge e of the electron as g=Q/e = C(Vbias-Vbreakdown)/e. For a 10x10 micron pixel, g~ (100 fF) x (few Volts)/e ~ 10^6. Generally, the doping more easily produces thermally generated carriers, and the high field region causes them to separate more easily, producing an amplified noise current. Fig. 10 shows typical pixel APD structure, from reference [xiii]. In effect, the APD appears as 3 resistor regions in series, with the thin middle resistor as the highest resistance, hence largest voltage drop, hence largest E in the region of the resistor[xiv]. Relatively little control is available for this resistance due to the doping needed. The designs for microAPD can be improved by extensive guard rings and field tapering to lower high E effects at edges, such that, in effect, “field emission” does not create more noise. .However, the technique remains limited by noise unless cooled. APD are often fully depleted over a thickness much deeper than the ~1 micron necessary for photon absorption, typically ~100 microns

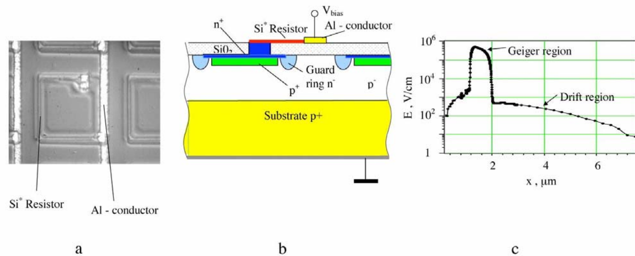

Fig. 10: a) Silicon PMT photomicrograph, b) topology, and c) electric field distribution in epitaxy layer (from Ref 14.)

or more (typical wafer thickness is 300 microns), specifically in order to reduce the large resulting capacitance if the thickness were left at ~1 micron. However, such a large bulk of “unused” silicon is therefore a source of thermally generated noise carriers. Our idea specifically reduces the volume of silicon by factors exceeding 100.

The technique described here was to use physical geometry produced by nanomachining to create a controlled high field region with a very limited amount of silicon in the high field region, and almost no doping. It would be made similar to a gas wire proportional radiation counter[xv], where the high electric field is only very near the fine wire, rising as E ~1/R as R-> wire diameter. The electrons from ion pairs created in the gas drift toward the wire, eventually producing an avalanche when (eE) x (electron-atom collision distance) exceeds the breakdown energy. The positive ions leave, creating a charge pulse on the wire. We recreate this in silicon. The difficulty with silicon as a medium to drift ions promoted into the conduction band as compared with an ionizable gas is that the silicon is by comparison highly conductive, and so a reverse bias diode structure is used to suppress a large bias current in which the signal would be lost. High purity lightly doped high resistivity silicon would be used to create a diode, with a narrow waist at the junction between n- and p-type. The photons absorbed in the p-type region would drift into the narrow waist of the junction. If the waist is ~1,000 times less in area than the p-contact (as reversed biased, the anode contact), then $E_{effective}$ in the waist is ~1,000x that of the saturated fully depleting drift field at the contact. If the field exceeds few x 10^5 V/cm, full avalanche breakdown occurs. This region of high field can be carefully controlled by the geometry of the silicon (outside of which is fully insulating), for example, making it as long as needed for impact ionization gain without the need for the full field for breakdown, lessening field-assisted thermal generation of carriers, controlling or limiting the avalanche, and making a smooth transition to higher fields without regions of very high field. Figure 2 shows a plot of the electric field from an array of point-like field shaping electrodes. Figures 4-5 show plots for the geometry and field similar to those of Fig. 1 shown for a normal doped-silicon APD. The great virtues of this approach is: a) the volume of silicon needed for the avalanche gain is ~100-1000 times less than in the planar doped diode, greatly reducing the region where noise carriers are most easily generated, and b) eliminating heavily doped silicon which has an effectively lowered interband bandgap, greatly increasing thermally generated carriers (exponential with the interband gap). Thus it is a reasonable expectation that lower noise APD could be created by silicon geometry, as the creator of high field impact ionization gain, rather than by doping alone. (This concept can of course also be combined with doped high field regions as well.) In general, to obtain pixels with a size in the 1-10 micron regime, nanomachining and nanofabrication/deposition techniques must be employed to make features in the high field region 30-1,000 times smaller than the pixel.

The basic idea bears a resemblance to the high field produced by silicon field emission cathodes, like the Spindt cathode [xvi],[xvii], shown in Figure 3, but in this case, instead of field emitting into vacuum, the electrons are “field-emitted” back into silicon across a junction – i.e. the avalanche is created by the high field created by the geometry, similar to that of a field emission cathode. This is close to a proof of principle, except for the issues of insulation. The existence of wire chambers, GEM, APD, and Spindt cathodes attest to the feasibility of the geometric high field approach.

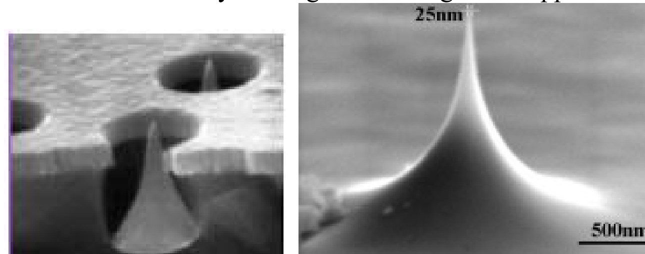

Figure 11: A gated “Spindt Cathode” and a silicon tip. As adapted herein, the field emission tip would “emit” back into a silicon junction, but as an avalanche. The tip terminates in silicon and the photoelectrons generated in the silicon would drift from the base silicon to the tip region where they would avalanche across the junction. Notice that the base and neck on the right are exactly in the correct ratio for a geometric APD.

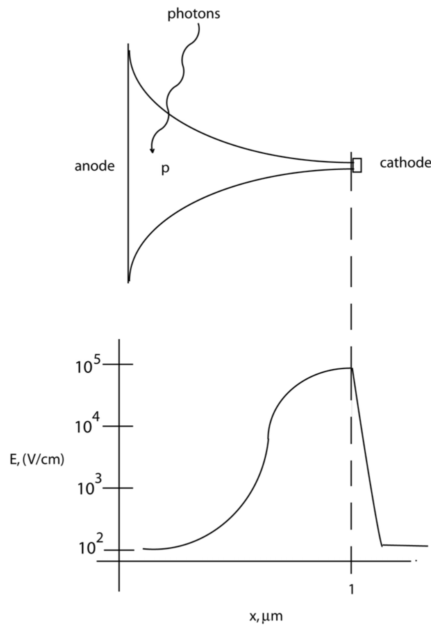

Figure 12: Geometric APD cartoon

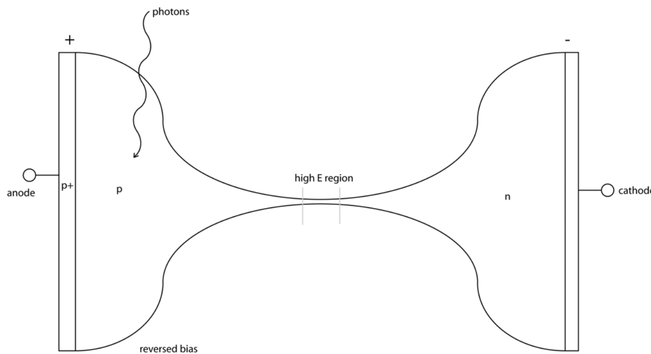

Figure 13: Plan-view of a Planar reverse biased GAPD "bowtie" geometry. The p-n junction is in the center. The geometric shape of the silicon concentrates the electric field in the neck at the junction at sufficient strength to cause either impact ionization gain or an avalanche compared to the drift regions in the p-type silicon. The length and shape of the silicon determine the gain properties. The thickness of the silicon can smoothly taper down from the electrodes to the center to further enhance the electric field. Typically the crossectional area of the neck must be ~0.001 of the area of the p-type electrode in order to develop an avalanche whilst still maintaining saturated electron drift velocities in the photon absorbing regions. The length of the high field region is between 0.1-1 micron long and the transverse dimensions between 10-30 nm. The very small volume of high field silicon and the absence of heavily compensated doped silicon reduces noise generation compared with standard APD. The region below the silicon and to the sides must be highly insulating.

A realization of this was made using p-type AFM tip, ~50 micron base x ~250 microns long, insulated by ~20 nm Si_3N_4 except the tip, with a metal annulus contact. The tip was placed by an STM/AFM to the surface of a polished thin n-type Si wafer, with a metal Ohmic back connector. A direct/anodic bond was made by a few microseconds HV voltage pulse. When the diode was reverse biased, and an intensity I of about 400,000+/-10% green photons/s from a 40 micron core optical fiber was applied on back annulus, the following resulted:

- 40 V, G>200, assuming QE 50%.
- 30-80 V, the Gain was linear within 20%
- 90~110 V, draws large current, Geigering.
- 110 V failed – we suspect heating or electromigration.

V. SUMMARY OF G-APD

This novel method of obtaining a Geometric APD[xviii]:

a) reduces the volume of the deleted region of silicon by factors exceeding 100, thereby reducing the amount of thermally generated noise, while preserving or lowering the output capacitance.

b) reduces interband dopants which generate thermal noise, nearly to zero.

c) allows the adjustment of the gain between the proportional and Geiger regime by both the gain channel length and area, as well as doping and applied voltage.

ACKNOWLEDGMENT

We acknowledge the many contributions of CP.Beets, R.Beorstlar, J.Steinbock, O.Siegmund, and A. Tresmin to parts of this work.

REFERENCES

[1] B.Sandel et al., Microchannel Plate Life Tests, Appl.Optics,Vol.16, 1435(1977)
[2] F. Bennett and D.Thorpe, Gain Degradation of Lead Type Channel Electron Multipliers in UHV, J.Phys:E, Vol 3, 241 (1970)
[3] C.P.Beets, R. Beorstlar, J. Steinbock, B.Lemieux, and D.R.Winn, "Silicon Micromachined Microchannel Plates", NIM-A, 442, p. 443-451 (2000)
[4] G. W. Tasker, J. R. Horton and J.J. Fijol, Materials Res Soc. Proc. 192, 459, (1990).
[5] G. W. Tasker and J. R. Horton, U.S. Patent 5,378,96 (1995).
[6] P. Sichanugrist, T. Yoshida, Y. Ichikawa and H. Sakai, J. Non-Cryst. Solids 164. 1081 (1993).
[7] W. T. Pawlewicz, J. Appl. Phys. 49, 5595 (1978).
[8] J. Sangrador, I. Esquivias, T. Rodriguez and J. Sanz-Maudes, Thin Solid Films 125, 79 (1985).
[9] G.Tasker et al., SPIE Proceedings V2640, 58 (1995)
[10] H.Seiler, Secondary Electron Emission, J.Appl.Phys.54(11), R1 (1983)
[11] J.Fijol et al., Secondary electron yield of SiO2 and Si3N4 thin films for continuous dynode electron multipliers, Appl.Surf.Sci 48/49, 464 (1991)
[12] G.Tasker et al., Thin-film amorphous silicon dynodes for electron multiplication, MRS Symp. Vol192, 459 (1990)
[13] P.Buzhan et al., An advanced study of Silicon PMT, ICFA Instrumentation Bulletin, 2002
[14] V.Golovin and V.Saveliev, Novel type of avalanche photodetector with Geiger-mode operation, NIM A518, 560 (2004)
[15] http://detserv1.dl.ac.uk/Herald/detectors_gas_detectors.htm
[16] P.R. Schwoebel, C.A. Spindt, C.E. Holland and J.A. Panitz, J. Vac. Sci. Technol. B 19(2), 2001
[17] W. Zhu, *Vacuum Micro-electronics*, John Wiley & Sons, New York (2001)
[18] D.R.Winn, US Patents Applied For. All Intellectual Property Rights Reserved.